Synthesis and Characterization of Platinum/GDC (Gd_2O_3-doped CeO_2) Dual-phase Membrane

Thesis

Presented in Partial Fulfillment of the Requirements for the Graduation of Honor Research Distinction in the Engineering School of the Ohio State University

By

Yi Zhou
Undergraduate Program in Engineering

The Ohio State University

2015

Dissertation Committee

Hendrik Verweij, Adviser

Michael Sumption

Abstract

Thin-film technology is attracting greater attention for its broad range of applications including oxygen separation, water purification, carbon capture, and solid state fuel cell (SOFC). In this study, ceramics membrane application in oxygen separation is investigated.

Oxygen applies to a broad variety of applications in science research and industrial processes, including primarily fuel combustion, metal processing, and medical uses. In particular with oxygen-enriched air combustion, efficiency is significantly enhanced. NO_x emission is reduced and carbon capture is simplified. Oxygen-enriched air production through membrane separation has attracted huge interest recently. An ultra-thin mixed-conducting dual-phase ceramic membrane was proposed to be a cost-effect design for oxygen separation. Thin-film (1μm thick) separation modules have exhibited promising permeance at low temperature (around 500°C). Low temperature (LT) operation also provides potential for less energy consumption. The synthesis feasibility and prospective are proved.

In this work, thin-film platinum/GDC (Gd_2O_3-doped CeO_2) dual-phase membrane was fabricated by colloidal processing. Colloidal synthesis was utilized to prepare nano-particle suspensions, followed by dip-coating and rapid thermal processing. α-Al_2O_3 substrate and mesoporous GDC layers were prepared to support Pt-GDC layer. To achieve density of Pt-GDC, electroless deposition (ED) process was studied. The effectiveness of electroless deposition is proved with scanning electron microscopy and X-rayiidiffraction. Thickness measurements by Spectroscopy Ellipsometry (SE) indicate a linear relationship between membrane thickness and number of GDC coatings.

Dedication

To my mom and dad,

And all of my beloved friends,

Without whom none of my success would be possible

Acknowledgments

My sincere gratitude first goes to my advisor, Prof. Hendrik Verweij, for providing me with the opportunity doing research under his instruction and guidance. I'd also like to thank Prof. Michael Sumption for being on my committee with insight and expertise.

I would also like to express my gratitude to Dr. Ioannis Mergos and Dr. Matthew Snider Dr. Minghui Qui, and graduate researcher Ralph Bauer who offered their generous help along the way.

Dr. Hong Zhou provided her knowledge and help with my questions in the process which was very helpful during I was writing this thesis.

Last but not least, my father and my mother have always supported me with kindness and love. With my deepest love, thank you.

Table of Contents

Vita

January 3, 1992…… Born- Chongqing, China

2015……B.S Materials Science and Engineering

List of tables

List of Figures

List of Symbols

XRD:X-ray diffraction
AKP30: Sumitomo Chemical α-Al_2O_3 powder with average $Ø_s$ ~ 300 nm.
EtOH: ethanol
ED: Electroless Deposition.
Pt: Platinum
Gd: Gadolinium
GDC: Gadolinium-doped Ceria ($Ce_{0.9}Gd_{0.1}O_{1.95}$).
MW: Microwave
PVA: Polyvinyl alcohol.
RTP: Rapid thermal processing.
SE: Spectroscopic Ellipsometry.
ED: Electroless Deposition

Ø: particle diameter

Chapter 1.

INORGANIC O2 TRANSPORT MEMBRANE

In this chapter, scientific background and state of art membrane for transport applications are discussed. Motivation for the work is introduced. Current designs for O_2 transport and for oxy-fuel applications, which is specifically the main application for this research, are illustrated. And important related content in literature is reviewed.

1.1 Background and Introduction

Oxygen applies to a broad variety of applications in science research and industrial processes, including primarily natural fuel combustion, metal processing, and welding processes. In an energy point of view, the use of oxygen-enriched air significantly enhances efficiency of combustion process, prevents NO_x emission, and simplifies carbon capture.

Existing oxygen production plants are based on cryogenic separation technique which capture all components all components of air. Novel oxygen membrane technology allows for production of oxygen with significant decrease in energy and economic cost. Membrane based oxygen-enriched combustion shows a net energy savings of 35% and a net economic benefit of 29% [1]. Production of high purity O2 by membrane technology also cuts tremendous energy consumption as shown in Figure 1.

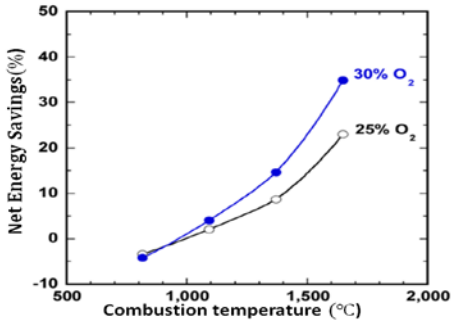

Figure 1: Effect of oxygen-enriched combustion on net energy savings at various combustion temperatures

More specifically, in coal-combustion electricity generation plant, the use of oxygen-enriched air provides the process with higher efficiency and lower emissions of nitrogen oxides [2]. Another instance is in the automobile industries. The power and efficiency is increased if the combustion engine is fed with oxygen-enriched air. This is similar to the application of turbo charger, which increases the oxygen density in the same amount of volume by compressing the inlet air. In a future area, oxygen enriched enrichment will be beneficial due to lower polarization losses on the cathode in fuel cell [3].

Industrial gas permeance membranes are characterized by measurements of gas permeability and selectivity, with gas selectivity being the permeability ratio of one gas over the other. Current studies have been focused on types of membrane materials including polymeric materials, ceramic membranes, dense metal membranes [2] and facilitated transport membranes [1]. However, these membranes are not as economically competitive as cryogenic distillation process of air for low selectivity and permeance. Additionally, for the O2 separation applications, membranes should be sealed and able to operate at relatively low temperatures (around 500°C).

500°C is relatively a low temperature limit compared to other designs currently under research. Cheng's group reported a 0.9 $\mathrm{ml \cdot min^{-1} \cdot cm^{-2}}$ at around 700 °C [4]. Serman J. Xu and his group reported limited oxygen permeation at 750 °C and promising oxygen permeation at 950 °C. State of art design and composition of oxygen transport membranes were aimed to perform at around 700 °C to 950 °C with maximized permeance [5].

1.2 Transport Mechanism

In this research study, thin supported ceramic dual-phase membranes are studied for cost-effective separation of O_2 from atmospheric air. O_2 is formed or incorporated at the external membrane surface in an exchange reaction written as $O_2 + 2e^- \rightarrow 2O^{2-}$. Specifically, surface chemical absorption of O_2 occurs on membrane surface, where oxygen molecules in air are absorbed as O^{2-} and desorb on the other side of the membrane

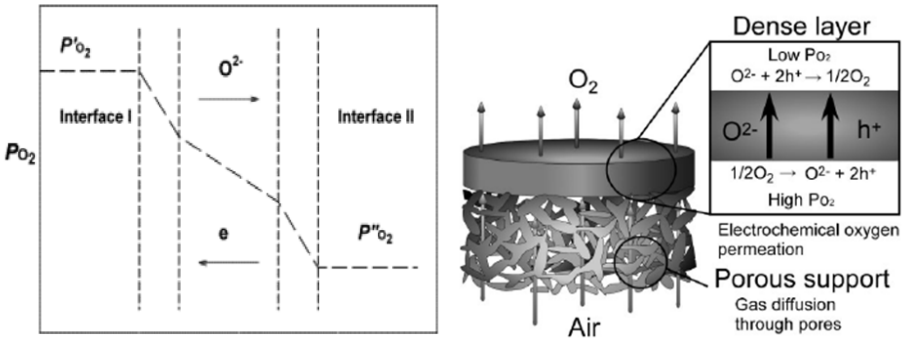

Figure 2: Dual Phase Oxygen separation membrane

as O_2. For some designs that made of materials which only provide ionic conductivity, electrodes need to be provided for electron transport to charge compensate the oxygen flux. Metallic or ceramic phase with superior electron conducting properties are proposed to be mixed into predominantly ionic conducting phase, which is an attractive pathway to the formation of dual-phase mixed ionic-electronic membrane.

The driving force of this design is the oxygen chemical potential gradient across the membrane. An illustrative drawing of the separation process is demonstrated in Figure 2 . $P_{O_2}^1$ and $P_{O_2}^2$ represent partial pressure of O_2 on the feed side and permeance side respectively. Figure 1.2 is another diagram that indicates the mechanism of the separation process, with chemical potential gradient of O_2 being the driving force, and electron movement keeping the charge of the whole system conservative.

A more detailed view of the transport mechanism is demonstrated in Figure 3. Three phases are present at the surface. They are electronic conducting phase, ionic conducting phase, and the gas phase. At the triple phase boundary, where three phases are in contact, surface reaction happens. In the reaction, one oxygen molecule splits into one O_2 and two e^-. At high temperature, bulk diffusions of O^{2-} and e^-.becomes significant and serve as means for O_2 transport. At the other side of the membrane, O^{2-} and e^- recombine into O_2 molecule.

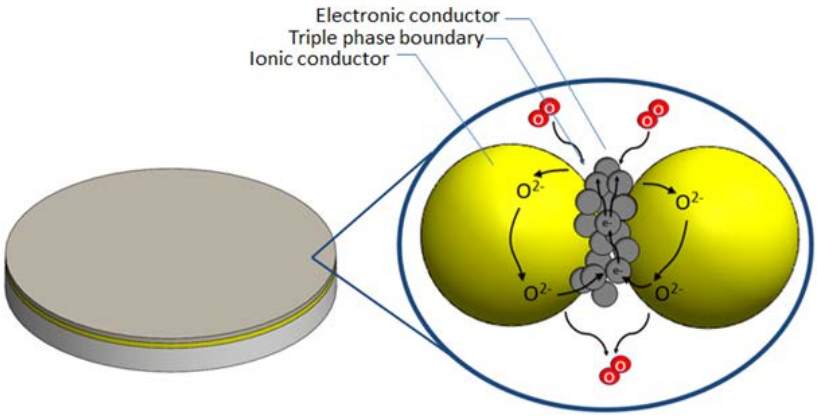

Figure 3: Concept view of mix-conducting in operation.

The effectiveness of O_2 transport is dominantly controlled by bulk diffusion and the surface exchange rates. It was reported that the oxygen permeation was dependent on pressure gradient as well as membrane thickness, which showed the permeation is controlled by both bulk diffusion of oxide ions as well as exchange kinetics between gas-phase oxygen molecules and oxide ions [5].

1.3 Membrane characteristics

The permeation and selection properties of membranes are controlled by the surface reaction process of the material in a microscopic view. They are also limited or affected by the macroscopic structure of the membrane. Thickness and pore size of the membrane are two important factors and characteristics for a gas transport membrane. For a thick membrane, bulk-diffusion is the limiting or determining step of the oxygen flux. Wagner theory describes the oxygen flux as:

$$J_{O_2} = \frac{1}{4^2 F^2 L} \int_{\mu_{O_2(2)}}^{\mu_{O_2(1)}} t_i t_e \sigma_t d\mu_{O_2}$$

$$t_i = \frac{\sigma_i}{\sigma_i + \sigma_e} = \frac{\sigma_i}{\sigma_t}$$

Where F is the Faraday constant, L is the thickness of the membrane, σ_i and σ_e are ionic and electronic conductivity. From this equation, it is clear that the oxygen flux is in inverse relationship with the membrane thickness. On other hand, the pore size controls the selectivity of the membrane. A dense membrane ideally has no pores in its structure. Without any open porosity for gas molecules to pass through in a ballistic mechanism, the selectivity of oxygen over other gasses, such as nitrogen and carbon dioxide, is maximized.

1.4 Literature Review

Currently, the most common oxygen production techniques include cryogenic air separation, and pressure swing adsorption-based systems (PSA). Since in cryogenic distillation process, feed air must be compressed and cooled down to −185 C, it is considered to be a complex, expensive and energy intensive process [7]. PSA utilizes a different mechanism from cryogenic air separation. Different material was used as adsorption agent causing nitrogen molecules in air to be adsorbed and hence separated. In the structure of zeolite, there exist non-uniform electric fields in voids or surface porosities, causing preferential adsorption of more polarizable molecules [8]. This makes pressure swing adsorption an efficient method for small scale oxygen production (20-100 tons/day), which is considerably smaller than cryogenic oxygen separation (100-300 tons/day) [7]. As a cost-effective alternative to traditional oxygen production processes, membrane technology can be applied with less amount of energy and produce oxygen-enriched environment in an efficient way. In addition, separation by oxygen membrane is simpler to operate and more reliable.

Current designs of oxygen permeation membrane include polymers and ceramics. For polymer membrane, selectivity of oxygen over other gases is less controllable since the polymeric membrane is porous and not being able to prevent other gas molecules other than oxygen from passing through the membrane. Ceramic membranes have attracted

huge interest in recent years for excellent oxygen permeance and ideally infinite selectivity.

For typical O_2 permeation membrane, the O_2 permeation flux should be equal or higher than 7.5×10^{-6} mol cm^{-2} s^{-1} [9]. Thus far, materials with dominant O^{2-} conductivity, such as fluorite-type oxides, had been examined. However, the electronic conductivities of these materials are at least two orders of magnitude lower than their ionic conductivities [9]. Then a second phase with high electronic conductivities was introduced. Acceptor doped CeO_2, specifically $(Ce,Gd)O_2$ is among the best known oxide conductors. The material finds use in catalysis and is also considered as an electrolyte, an electrolyte barrier layer, and an electrode backbone layer in solid oxide fuel cells (SOFCs) [10]. Examples of ion-conducting compounds include δ Bi_2O_3 (rare earth doped) [11], cubic Yttrium-doped zirconia (YSZ), and $GdCe_xO_y$ (GDC). δ Bi_2O_3 has the highest ionic mobility but is unstable. YSZ has the lowest mobility but is very stable. CGO has a better ionic mobility than YSZ but is less stable and somewhat mixed conducting. The latter makes that GDC cannot be used as a fuel cell electrolyte but is still very suitable for the dual phase membrane. Noble metals such as Ag and Pt are the first choice for the electron conducting phase. They do not react with the electrolytes and have a high catalytic activity for the O2 surface transfer reaction. Ag is less preferred since it oxidizes at low temperature, and is volatile at operating conditions. Its melting point of 962ºC is too close to maximum operation temperatures which increases the risk of surface-tension induced rearrangement [12].

Chapter 2.

DESIGN AND MATERIALS OVERVIEW

In this chapter, an overview of the design and the materials are introduced.

2.1 Objective and Design Overview

The objective of this project is to prepare dense supported nano-composite membranes for high performance O_2 separation at >500°C with an apparent O_2 permeance. The objective is expected to be achieved this by producing thin, dense, nano-composite dual-phase membranes on a smooth, strong and permeable support, shown in Figure 4. In this approach a clear separation between the membrane function and structural support properties was realized. The percolative membrane phases are either electron- or oxygen ion-conducting. The synergy between both phases provides a fully selective net O_2 transport in a chemical gradient (see Figure 4). The nano-structure is needed to provide sufficient active interface in the bulk and a high concentration of active sites (triple phase boundaries) for O_2 surface transfer. The proposed combination of properties is a major step forward, compared to the state-of-the-art.

In order to cut down the temperature limit and enhance the permeance of the membrane, an ultra-thin Pt-GDC dual phase membrane is proposed. The membrane is designed to be a three-layer structure of gradually decreasing thickness and increasing pore size was used. As shown in Figure 7, the macroporous layer has pore diameter Ø >50nm, the mesoporous GDC layer has 2 < Ø <50nm, and the top Pt-GDC layer is dens and ideally has no pores extrinsic to its crystal structure [14]. The layers configuration is dense Pt-GDC layer, mesoporous GDC layer, and macroporous support layer respectively from top to bottom. In order to form a homogeneous and defect-free surface for the Pt-GDC layer, colloidal method was applied for preparation of AKP30 α-Al_2O_3 support.

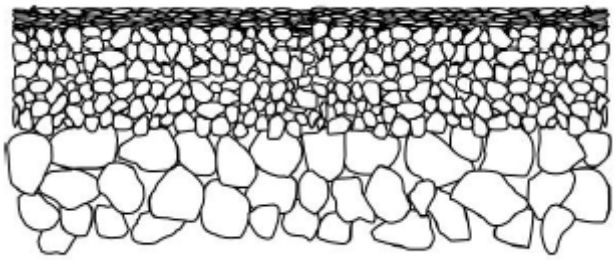

Figure 4: Schematic drawing of the membrane design.

2.2 Introduction to $Gd_{0.1}Ce_{0.9}O_{2-\delta}$ (GDC) and platinum

Gadolinium doped ceria (GDC) has a fluorite structure as indicated in Figure 5. Gd^{3+} is introduced into the structure as Gd_2O_3. Kilner's research group confirmed that the CeO_2-Gd_2O_3 system has the highest ionic conducting ceria based binary system [15]. Specifically, the ion conductivity is maximum for Gd^{3+}, the radius of which is almost exactly equal to that of Ce^{4+}. It is clear that the ionic conductivity is affected by the addition of Gd^{3+} ion and the oxygen vacancy. Figure 6 is a graph of the effect of dopant level on ionic conductivity [16]. It is indicated that at around 10% Gd^{3+} content, GDC reached the highest ionic conductivity. Also, Gd^{3+} has significantly higher conductivity than La and Yb. This is explained that the ionic conduction is affected by the mismatch in size of the dopant ion and the original ion. When the mismatch happens, elastic strain is introduced into the lattice and it further affects the interaction of the point defect (vacancy).

As a result, 10% Gd^{3+} is to be used and the investigation of the synthesis method is to be discussed.

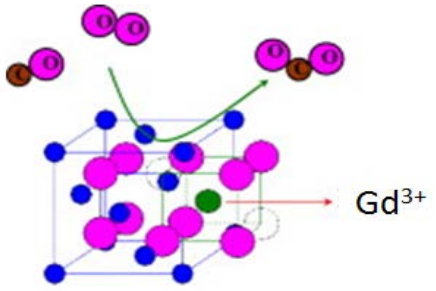

Figure 5: Concept view of mix-conducting in operation.

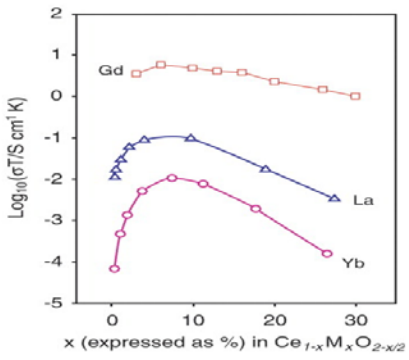

Figure 6: The effect of dopant level on ionic conductivity.

As another phase of the dual-phase structure, platinum as a noble metal as discussed in chapter 1, is chosen to be the electronic conducting phase. This is because Pt has a melting point at 1768.3°C, while silver has a melting point of 893°C, which could be unstable at operating temperature of oxygen membrane. Also, another concern is the thermal expansion coefficient. As shown in Figure 7, the thermal expansion coefficient of $Gd_{0.1}Ce_{0.9}O_{2-\delta}$ is around 10^{-6}/K at room temperature. Significant difference in thermal expansion of the two phases could lead to cracks and mechanical failure. A shown in Table 1, platinum has the highest melting point and relatively identical thermal expansion coefficient.

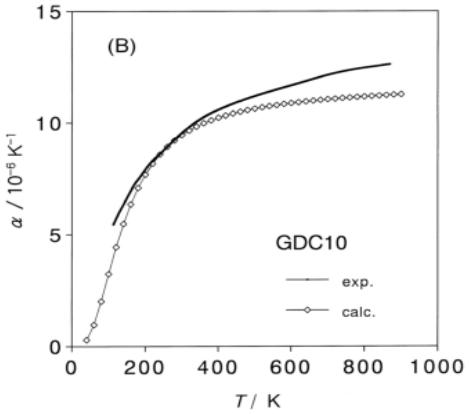

Figure 7: Thermal expansion coefficient of GDC

Table 1: Thermal expansion coefficient (20°C) and melting point of materials

	Platinum	Gold	Silver	Copper
Expansion (10^{-6}/K)	9	14	18	17
Melting Point (°C)	1768.3	1064.18	961.78	1084.62

Chapter 3.

EXPERIMENTAL

In this Chapter, the major preparation and synthesis methods that included in the research are introduced. The fabrication methods are referenced to the Inorganic Materials Science Group.

3.1 α-Al_2O_3 supports preparation

α-Al_2O_3 is used as a macroporous supporting substrate for the functional Pt-GDC layer, and it is prepared for subsequent dipping of intermediate GDC layer and Pt-GDC layer. To prepare α-Al_2O_3 supports, colloidal methods are used to enable production of homogeneous porous ceramic substrate. Colloidal methods provide controlled particle size for the application of thin defect-free membranes. In this research study, AKP30 α-Al_2O_3 powder is dispersed in water by focused ultra-sonic treatment with HNO_3 as a charge-stabilizer. The dispersion is screened with a fine nylon mesh to remove coarse agglomerates and contamination. Disk-shaped filter cakes are then obtained by pressure filtration of the dispersion in a custom-made manifold. The compacts are sintered in the surface-diffusion controlled regime such that necks are formed between the particles for inorganic membrane support applications. A top view SEM is shown in Figure 8.

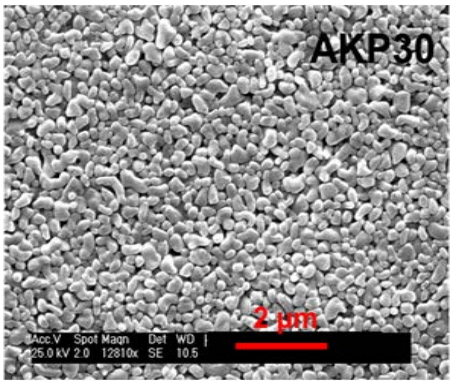

Figure 8: SEM imgage of α-Al_2O_3 powder

3.2 Synthesis of Gadolinium Doped Ceria ($Gd_{0.1}Ce_{0.9}O_{1.95}$) dispersion

As discussed in Chapter 2, gadolinium doped ceria (GDC) was one of the materials used in the intermediate and the top dual-phase layers. Sonochemical method is used for synthesis of GDC dispersions. Sonochemical synthesis is used to make stable colloids of ceria and gadolinium doped ceria (GDC) for applying thin meso-porous membranes on ceramic supports. Stoichiometric amounts of cerium and gadolinium precursors are added to water, and treated by a focused ultrasonifier. Addition of TMAOH during ultrasonification facilitates the GDC synthesis reaction. Addition of bicine aids in creating and maintaining a uniform dispersion. The resulting colloid is dialyzed to remove nitrate as well as to reduce the pH to further stabilize the dispersion. In this project, $Gd_{0.1}Ce_{0.9}O_{1.95}$ was used as discussed in Chapter 2 that a stoichiometric compound of $Gd_{0.1}Ce_{0.9}O_{1.95}$ has the optimum ionic conductivity. Specifically, The cerium and gadolinium precursors, (cerium ammonium nitrate $(NH_4)_2Ce(NO_3)_6$, gadolinium nitrate hexahydrate $Gd(NO_3)_3 \cdot 6H_2O$,) are used. A digital sonifier is used to generate the required energy for the synthesis reaction as well as mixing the reactants and dispersing the product particles. Another goal of the sonification process is to break down large nucleation or agglomerates with the dispersion of energy that the sonifier produced. A dialysis process is followed to remove the salts from dispersion as well as to lower the dispersion pH of 2. Table 2 shows the optimized GDC formulation for the membrane synthesis in terms of stability and particle size. The Pt-GDC dip solution was made by mixing the GDC colloid with Pt suspension in a 1:1 volumetric ratio and addition of 0.7 ml EtOH.

Table 2: Optimized formulation for 8.5wt% GDC colloid

Material	Amount
Ce precursor	16.2±0.1 g
Gd precursor	1.481±0.01 g
Water	28.3±0.05 ml
TMAOH	20.4±0.05 ml
Bicine	0.268±0.01 g
pH after dialysis	2.1

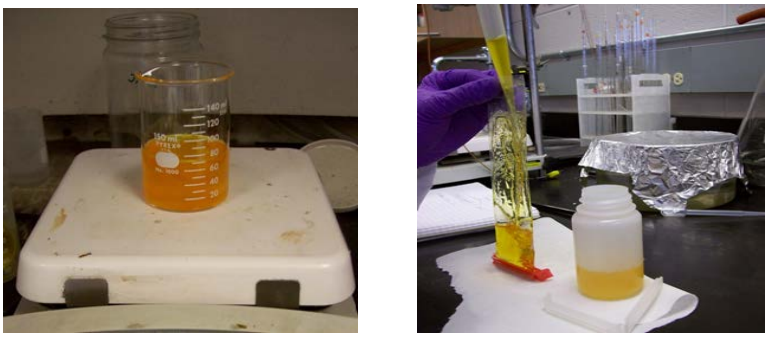

Figure 9: Precursor dispersion for $Ce_{0.9}Gd_{0.1}O_{1.95}$ on a stir plate (left) and dialysis process of the GDC dispersion (right)

3.3 Synthesis of Pt suspension

Platinum suspensions were prepared from choloroplatinic acid hexahydrate ($H_2PtCl_6{\cdot}6H_2O$) by wet chemical synthesis. Choloroplatinic ion is reduced by methanol with the following reaction formula:

$$PtCl_6^{2-} + CH_3OH \rightarrow PtCl_4^{2-} + HCHO + 2H^+ + 2Cl^-$$

$$PtCl_4^{2-} + CH_3OH \rightarrow Pt + HCHO + 2H^+ + 4Cl^-$$

Table 3: Optimized formulation for 3mM Pt suspension synthesis

Material	3mM Pt Colloid
$H_2PtCl_6{\cdot}6H_2O$	0.034 ±0.001 g
3wt% PVA	11.4 ±0.1 ml
Methanol	8.6 ±0.05 ml

The reaction happens at 85°C for 4 hours while stirring on a hot plate. 3wt% polyvinyl alcohol (PVA) (hydrolysis 99.3%; viscosity 28-32cps) is required for this synthesis as steric stabilizer that prevents the platinum particle from aggregation and sedimentation. Two platinum concentrations are produced to study its effect on performance of the membrane. Platinum dispersion is then mixed with GDC colloid with a certain volumetric ratio for the coating of Pt-GDC top layer.

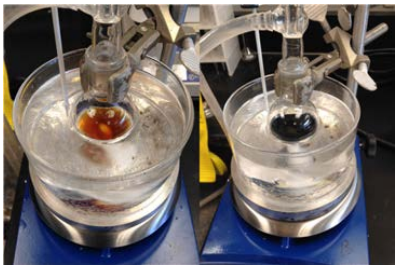

Figure 10: Platinum suspension in oil bath. (Left) Orange color at beginning of synthesis. (Right) Black color at conclusion of synthesis.

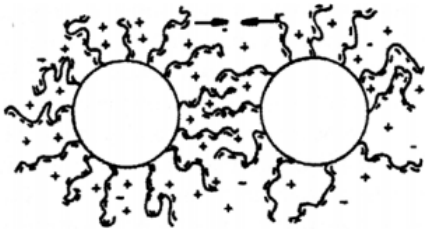

Figure 11: Schematic drawing of steric stabilization

3.4 Dip coating

Dip coating is one technique that controls precisely the depositing a layer of material by immersing and withdrawing a substrate into a suspension of small particles. As shown in Figure 12, α-Al_2O_3 is immersed into the dipping solution while it rotates from the top to bottom. In this research, the dipping solutions are GDC and Pt-GDC. The thickness of the membrane coated could be maintained uniform and controlled with the deposition speed and solution viscosity. To produce a dip-coating suspension for Pt-GDC membrane, a

mixture of 1:1 Pt and GDC suspension was produced. The suspension was filtered through 3 μm filter.

Specifically, two layers of intermediate coating and one layer of Pt-GDC coating are dip-coated on α-Al_2O_3 substrate. After each coating process, the membrane is dried at 110°C for 1 hour to remove liquid and organics from the colloid suspension. Then the membrane is ready to be rapid thermal processed.

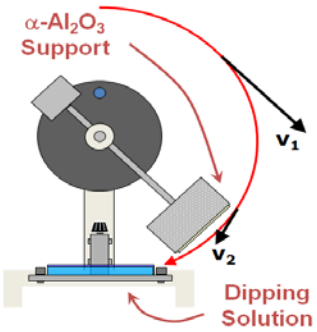

Figure 12: Schematic drawing of dip coating machine.

3.5 Rapid Thermal Processing

One advantage of Rapid Thermal Processing is that RTP can be used to reduce thermal redistribution of impurities at high temperature [17]. For dense thin film membranes applications, surface impurities could directly affect the performance of the device. Hence RTP process is used to process the membrane after each coating. The dip-coated samples were dried at 110°C for 1 hour. The Rapid Thermal Process is carried out in a Modular Process RTP-600x device with a heating rate of 10°C/s for 3 minutes. As shown in Figure 13, halogen lamps disperse massive radiative energy directly onto the sample and the silicon wafer. This process is much faster and more effective than traditional thermal processing.

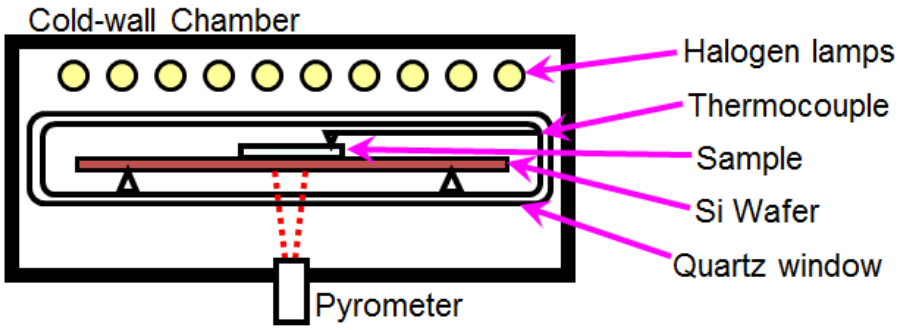

Figure 13: Schematic drawing of RTP machine

3.6 Electroless Deposition

Electroless deposition has been used in industry and research for coating different types of materials, including metals or alloys. It is also noted that the electroless deposition of oxides, salts, polymers is also possible [20]. As reduction of $PtCl_6^{2-}$ happens in the solution, Pt particles nucleates and will grow to form a crystal. For nucleation, heterogeneous nucleation is more likely to occur than homogeneous nucleation. In the electroless deposition process, Pt that is already imbedded inside the Pt-GDC membrane serves as a nucleation seed. Nucleation is more likely to happen at the seed particle because it diminishes the free energy barrier. As mesoporous Pt-GDC layer is formed, densification is needed in order to maintain an oxygen partial pressure difference and keep high selectivity.

$$PtCl_6^{2-} + N_2H_4 \rightarrow Pt + N_2 + 4H^+ + 6Cl^-$$

As shown in the above formula, Pt particles will be formed by reduction of $PtCl_6^{2-}$. Nucleation is expected to happen inside the mesoporous structure. Densification process is complete ideally when all the open porosities are closed. In the meantime, the amount of Pt deposited on the membrane is controlled to ensure that the surface will not be covered completely by Pt particles. This is because when an entire plating of Pt is formed , surface reaction of O_2 is disabled since phase boundaries between GDC and platinum on the surface would be isolated from atmospheric air. Table 4 is an optimized electroless deposition solution formulation.

Table 4: Optimized formulation for electroless deposition process

Materials	Amount
$H_2PtCl_6 \cdot 6H_2O$	100 mg
Hydrazine (N_2H_4)	250 µL
Water	45 mL
EDTA	6.22 g
NH_4OH	5 ml

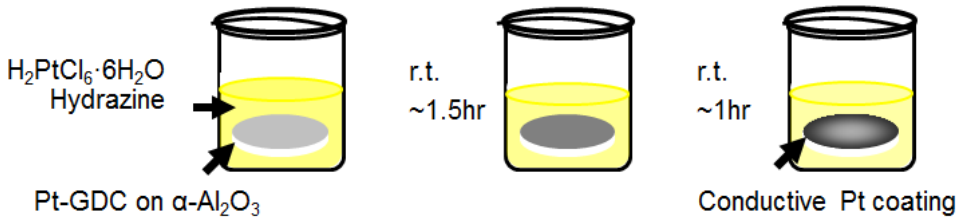

Figure 14: Electroless deposition process

3.7 Gas permeation measurements

The permeation test in this research is performed in a Wicke-Kallenbach cell, see Figure

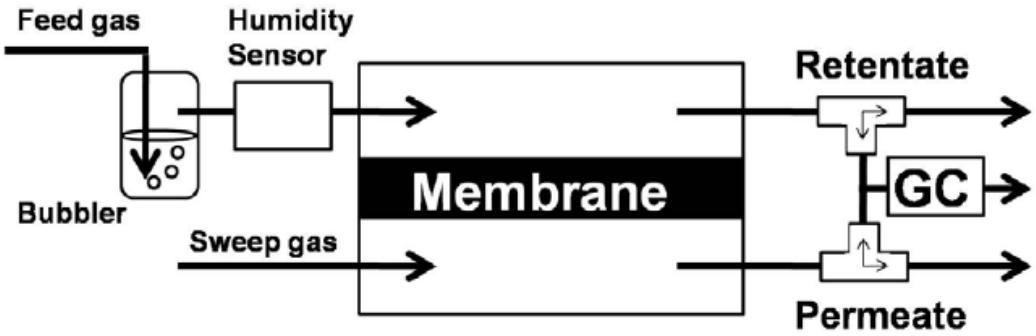

Figure 15 Gas Permeance test (separation) setup [18]

15. The Wicke-Kallenbach cell consists of two compartments separated by the

membrane. A steady gas stream with certain composition flows through one compartment, while the other stream of inert gas flows through the other compartment as a sweep gas [19]. The flow rates of feed and sweep gas is controlled by mass flow controller. The feed gas flow and the helium sweep flow were 100sccm. To simulate gas content in atmospheric air, the feed gas contains 80sccm N_2 and 20sccm O_2.

Chapter 4.

FINDINGS AND DISCUSSION

In this chapter, results and major findings throughout the research are presented. Related knowledge and understanding are discussed. This chapter also includes problems encountered in some processes with explanations and solutions.

4.1 Colloidal stability

Colloidal stability is firstly affected by sedimentation effect. Earth gravitational force pulls the particles with a force of $G = mg$, in which m is the mass of the particle and g is the gravitational acceleration. For particles with a diameter smaller than 1 nm, the Brownian motion becomes a major factor and the sedimentation effect is less significant.

Colloidal particles constantly show Brownian motion that leads to particle collision and coagulation. Other forces, like convection and gravity can also cause collision. Agglomerates or coagulation of particles could possibly form if particles are brought together and Van der Waals force becomes significant enough to attract them. The colloid is destabilized when large amount of aggregates are formed.

Three major mechanisms in colloidal stabilizations are electrostatic stabilization, steric stabilization, and electrosteric stabilization. In electrostatic stabilization, a surface charge layer is formed around particles which creates a repulsive force and counteracts the Van der Walls attraction. In some cases, colloidal particles could be stabilized by steric stabilization. This is achieved by polymer molecules that attached themselves to particle surface, see Figure 16. The polymer chains are attached to colloid nanoparticles with one end and the other end dispersed in the solution. The dispersed ends create physical barriers that prevent particles from colliding with other particles.

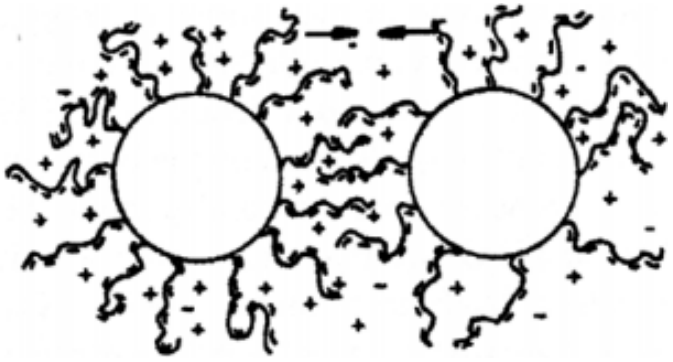

Figure 16 Schematic drawing of steric stabilization.

4.1.1 $Gd_{0.1}Ce_{0.9}O_{1.95}$ (GDC) colloids

The particle size distribution is critical to the membrane layer homogeneity, pore size and eventually dense composite membrane properties. The particle size distribution of thus prepared GDC dispersions was measured with Dynamic Laser Scattering (DLS) the result is shown in Figure 17. As described in Chapter 2, the sonification process aims to produce energy to break down agglomeration and maintain a uniform particle size in the dispersion. Consequently, the duration and the intensity of the sonification treatment are two methods to modify the particle size distribution. Changing the treatment time from 8 minutes to 15 minute will decrease the maximum $Ø_p$ (particle diameter) from 15 nm to

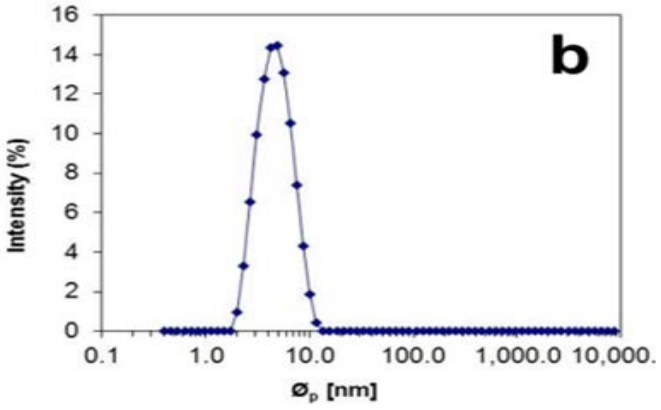

Figure 17 DLS scattering intensity vs particle size, $Ø_p$, for 8.5 wt% CGO precursor sol.

4 nm. After the sonification process, the excess nitrate salt in the GDC colloid could possibly reacts with other additives in the colloid process. Another effect is the combustion of nitrite salt during heat treatment of the membrane while the expansion in gas volume would cause collapse or the membrane. Hence a dialysis process is performed to remove the salts from dispersion as well as to lower the dispersion pH of 2.

4.1.2 Pt suspension

As introduced in Chapter 3, platinum suspension is prepared by wet chemical synthesis. Platinum suspension is stabilized by steric stabilization with PVA (polyvinyl alcohol). One observation made during the storage of Pt suspension is the gelation effect, see Figure 18. The platinum suspension could be stored up to 2 months after synthesis and eventually will be destabilized with the gelation effect. As shown in the picture, suspension has been divided into two layers, with a clear top layer of water.

Figure 18: Gelation effect of Pt suspention (left)

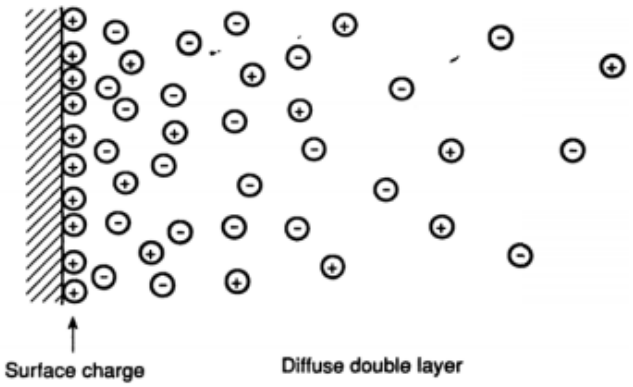

Figure 19: Surface charge layer and diffusive double layer.

One possible explanation for this effect is as follows. A highly acidic environment will be formed as the synthesis reaction happens with the product of H^+. Also, oxidation of methanol creates carboxylic acid (COOH). Platinum particles absorb H^+ as a surface charge layer and form (PtH^+) core. Carboxylate ion (COO^-) is in the diffusive double layer. $(PtH^+)_m$ further reacts with (COO^-) in the diffusive layer, forming a $[(PtH^+)_m(n\text{-}x)\ COO^-]^{m\text{-}n\text{-}x}$ structure. When the a $[(PtH^+)_m(n\text{-}x)\ COO^-]^{m\text{-}n\text{-}x}$ is growing, the attractive force between this particle and PtH^+ passes a threshold value and contract the repulsive force created by PVA's stabilization effect. At this point, a cross-linking structure among (PtH^+) particles is formed.

If the gelation explanation is valid for the synthesis of Pt suspension by methanol oxidation, the problem could be resolved by adjusting the methanol amount that leads to complete reaction. Also, reduction of $PtCl_6^{2-}$ by H_2 could possibly be another solution.

4.2 Membrane analysis

4.2.1 Membrane Microscopy

To visually analyze the characteristics of each membrane layer, optical pictures were taken after each coating. Since in the Pt-GDC layer, a dual-phase structure of Pt and GDC is formed, the membrane shows a dark brown color. As seen in Figure 21, a clear Pt phase, exhibited in black, has been successfully imbedded into the GDC phase.

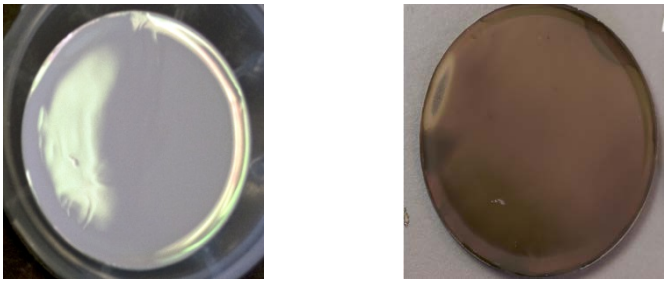

Figure 20 Pictures of GDC intermediate layer (left) and Pt-GDC top layer (right)

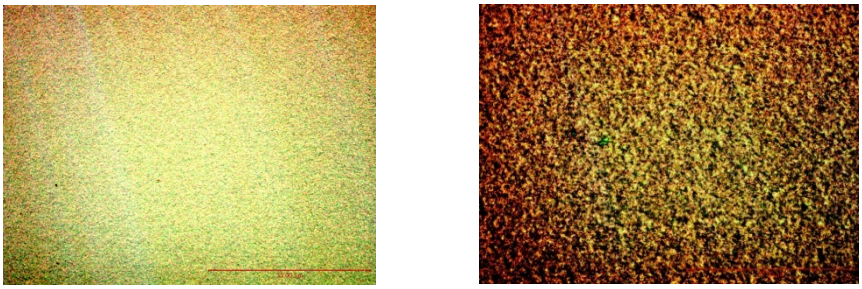

Figure 21 Optical Microscopy of GDC intermediate layer (left) and Pt-GDC top layer (right)

SEM image of Pt-GDC layer was taken using secondary electron detector, see Figure 22. The image reveals a homogeneous surface with some defects as indicated in the figure. The defects could be dust particles or agglomerates in the GDC colloids during the dip coating process.

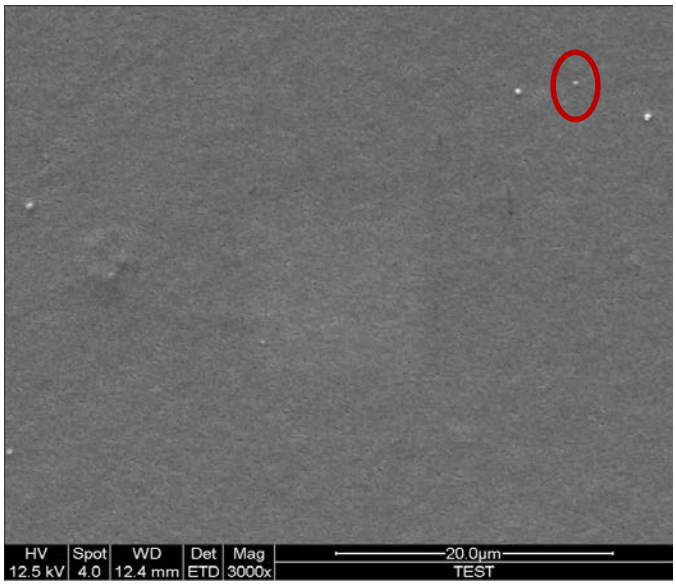

Figure 22 SEM image of Pt-GDC layer using secondary electron detector

As described in Chapter 3, a dense top structure with ideally no porosity is required to achieve optimum selectivity. A dense top membrane blocks gas molecules other than O_2, for example N_2, CO_2, from passing through the membrane. This also helps maintain a steady pressure difference which is the driving force for O^{2-} diffusion through GDC phase. However, a back-scattered electron detector shows a porous top structure, as shown in Figure 23. The area of pores of the top layer is analyzed with a binary graph of the same picture. The analysis reveals that the surface of the top Pt-GDC is covered with pores with a surface area of 10.63%. Although the binary graph is not an exact simulation of pore structure and hence could not accurately calculate the pore area, it demonstrates that the top layer has significant amount of pores.

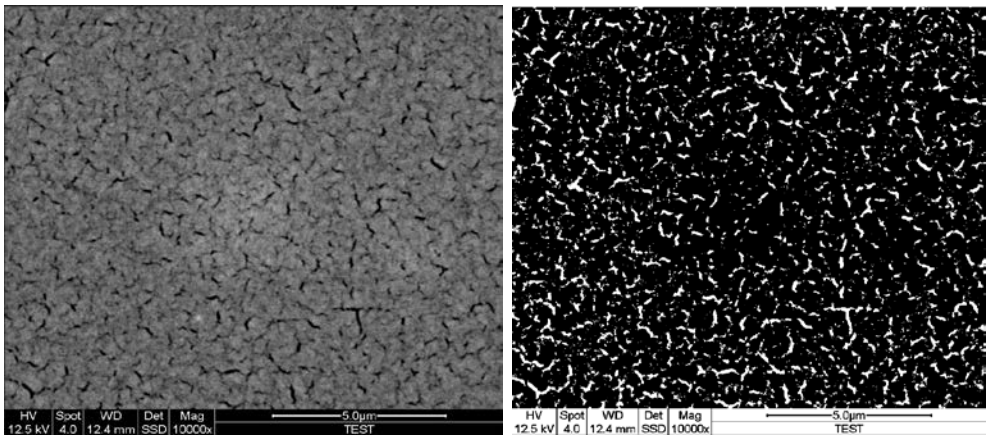

Figure 23 SEM image of Pt-GDC layer using back-scattered electron detector (left) and the binary transition of the image

With pores being identified, SEM images of membrane after electroless deposition were taken see Figure 24. Also as discussed, eletroless deposition process is designed to fill inside the pores. Nucleation and particle growth inside the pores are expected to facilitate pore filling effect. As a comparison to Figure 22, large amount of Pt particle deposition is observed. These particles have a diameter range from around 100 to 500 nm. Also, as the red circle in Figure 24 indicated, platinum islands are formed on the membrane surface. The fraction of surface area covered by platinum particles and platinum islands is 11.02%. As a result, the deposition of platinum particles and islands creates significant amount of surface area. Since the surface reaction happens at the triple phase boundary, addition of surface area could potentially enhance the efficiency of the surface reaction given more triple phase boundaries are created. This property is yet to be proved since triple phase boundaries could also be covered and lead to a reduction in efficiency.

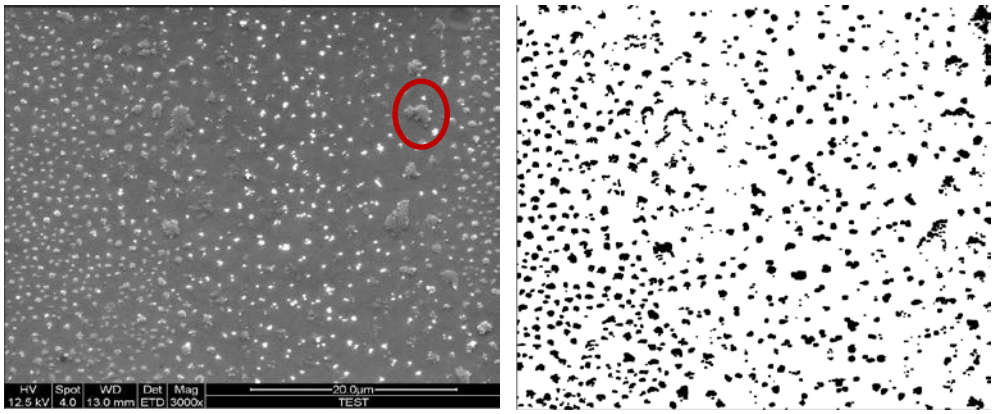

Figure 24 SEM image of Pt-GDC layer using secondary electron detector (left) and the binary transition of the image (right)

To closely study the pore filling effect of the electroless deposition process, SEM images of back-scattered electron detector was taken, see Figure 25. Compared to the membrane surface of Pt-GDC before electroless deposition in Figure 23, the membrane shows a relatively smooth and pores-free structure, which is evidence that proves a dense top Pt-GDC layer.The area circled in red is one of the platinum islands that extruded from the surface.

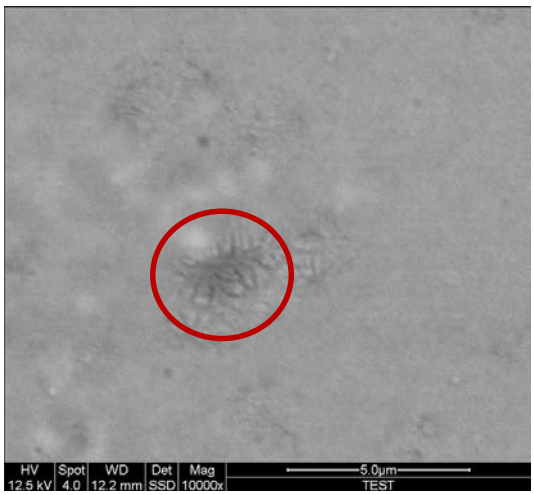

Figure 25 SEM image of Pt-GDC layer after electroless deposition using back-scattered electron detector

As duration of the electroless deposition process is one factor that controls that amount of Pt that is deposited on the membrane surface, time effect on the electroless deposition process is investigated. Three time length of electroless deposition processes were performed on three Pt-GDC membranes. Table 5 exhibits the time effect on the results of electroless deposition process. The optimal electroless deposition duration according to the table is around 2 hours.

Table 5: Time effect on electroless deposition process

Time length	Deposition status	Membrane status
2 hrs	Pt particles/ few Pt islands	Intact
4 hrs	Massive Pt islands	Intact
5 Hrs	Pt dendrites	Intact
12 hrs		Peeled off

Figure 26 shows a representative picture of platinum dendrite. As indicated in the image, Pt dendrites have grown into dendrite structures and formed a Pt coating covering the whole local area. As discussed in Chapter 2, Pt nucleation has higher possibility to happen heterogeneously at sites where Pt nucleation is already formed. This leads to an exponential growth of Pt precipitations.

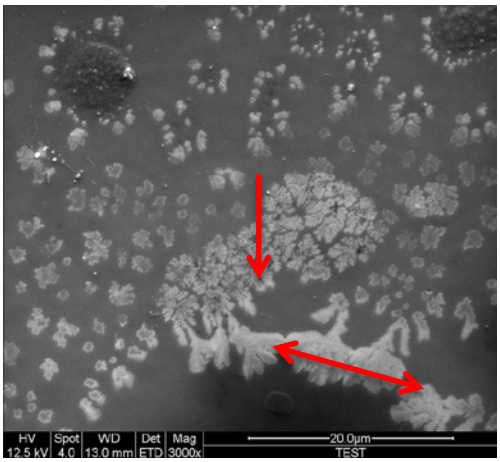

Figure 26 SEM image of Pt Dendrite taken using secondary electron detector

However, the deposition process is controllable with a pattern shown in Table 5. The optimized treatment time is around 2 hours. The process could also be controlled in coordination with the reactants concentration. The optimal combination of these two effects is of interests for further study.

4.3 Thin film XRD characterization

The crystalline characteristics of GDC, Pt-GDC, and ED-PtGDC can be seen in Figure 27, in which all peaks of platinum phases and the GDC phases are identified. For the platinum phase, the peaks at 39.76 °and 39.82 ° are the characteristic peaks of (111) plane for platinum of Pt-GDC sample and ED-PtGDC sample. Other peaks at 46.36 ° and 47.28 °respectively for Pt-GDC and ED-PtGDC are observable as indicated. Compared to XRD result of GDC sample, these unique peaks of platinum are indications of existence of platinum phase. However, only two peaks of platinum are observable. This is because of low platinum content in the dual-phase structure. For the GDC phase, one characteristic peak is at around 28.5 ° for three XRD diagrams. The crystallite size (grain size) of Pt phase and GDC phase are calculated using the characteristic peaks using Scherrer Equation below:

$$\tau = \frac{K\lambda}{\beta cos\theta}$$

Where τ is the mean size of ordered (crystalline) domain, K is the asymmetric factor, λ is the X-ray wave length (0.154 nm), β is the broadening at half of the maximum intensity (FWHM), θ is the Bragg angle. The Scherrer equation could only be used to qualitatively analyze the crystallite size because the broadening of peaks in XRD is also affected by grain boundaries, defects. According to calculation, crystallite sizes of GDC and platinum stays relatively the same for three samples. For platinum after electroless deposition specifically, crystallite size does not change much given the inaccuracy of the Schereer calculation. However, this result indicates that the electroless deposition process did not form platinum plating covering the surface.

Table 6: Crystallite Size by Scherrer Equation

Phase	Sample	Crystallite Size (nm)	Bragg Angle (rad)	FWHM (rad)	Asym. factor
Platinum	ED-PtGDC	12.901	0.693	0.015	0.9955
	PtGDC	14.497	0.694	0.014	1.0359
GDC	GDC	7.822	0.497	0.020	0.908
	PtGDC	6.433	0.575	0.024	0.8307
	ED-PtGDC	5.972	0.497	0.030	1.0354

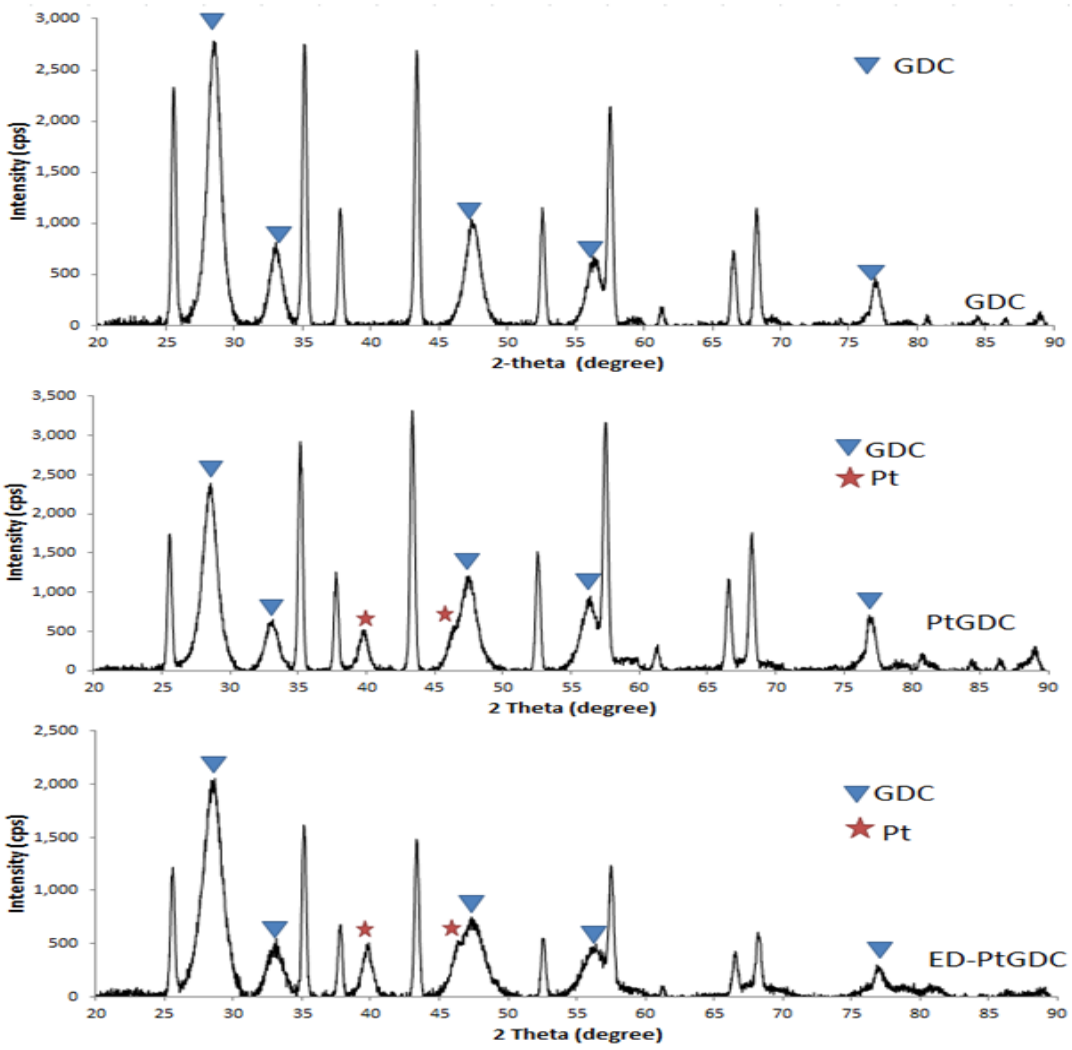

Figure 27: XRD pattern of GDC, PtGDC, and PtGDC after electroless deposition

4.4 Thickness measurements

Membrane thickness measurements were taken by spectroscopy ellipsometry (SE). Ellipsometry provides a means to understand physical properties on the material of interest by analyzing optical information reflected from the sample. Standard ellipsometry is used for characterizing thickness or optical properties of bulk or layered materials [21]. After obtaining the measurement data, modeling analysis was performed by a fitting of a Cauchy layer. Representative ES measurements for GDC layer and Pt-GDC layer and corresponding fitting of these measurements are shown in Figure 28.

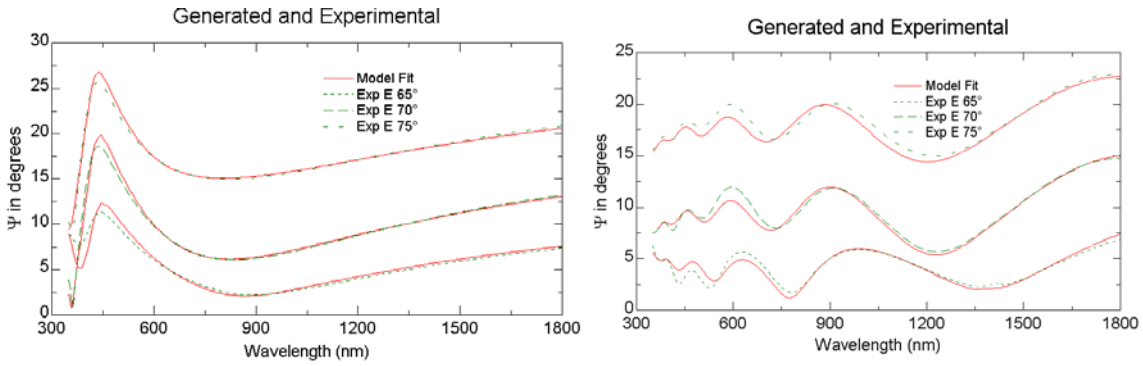

Figure 28 Representative SE measurements for GDC layer (left) and Pt-GDC layer (right)

To study how number of intermediate GDC coatings affects the thickness of the membrane thickness. Three sub-layers of GDC coatings have been deposited consecutively. The membrane thickness was measured each time after one coating.

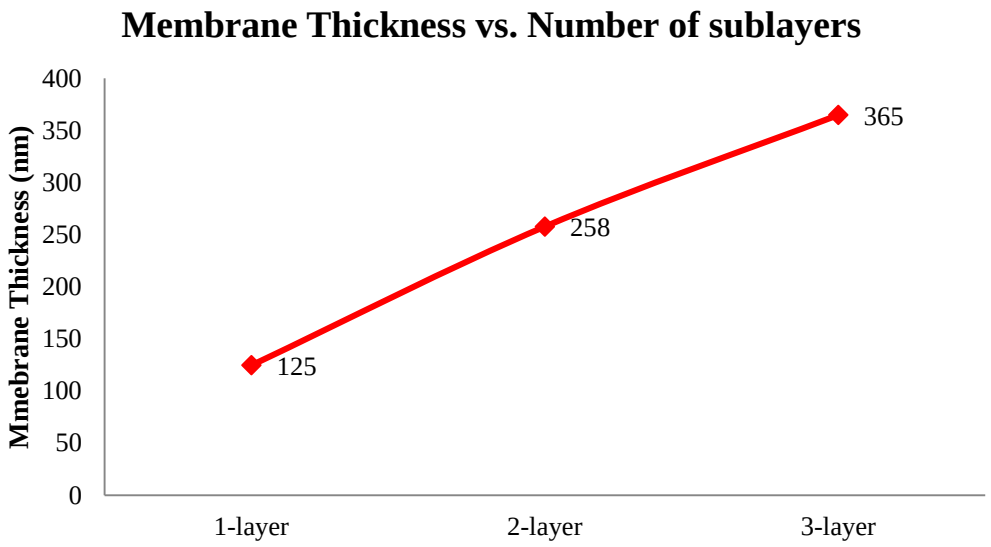

Figure 29 Thickness measurement of intermediate GDC layer

The membrane thickness is 125 nm, 258 nm, and 365 nm after 1, 2, and 3 coatings respectively. As Figure 29 shows, the membrane thickness almost exhibits a linear relationship with number of GDC coatings.

For Pt-GDC layer, as discussed in Chapter 1, oxygen permeance is inversely related to the thickness. Characterization of the Pt-GDC;GDC;AKP30 structures was generally difficult, both because of the large total number of layers involved, and due to the nature of the Pt-GDC layers. These are partly metallic and besides high dielectric constant, usually have significant optical absorption that attenuates the transport of radiation from lower layers and hinders thickness calculations. After RTP, the single Pt-GDC coatings had thickness > 200 nm, significantly higher (sometimes more than double) than the single GDC coatings.

To achieve optimal performance of the membrane, thinner membrane thickness is more preferable. It appears that a single coating of Pt-GDC provides a layer of adequate thickness, and a second coating is not needed.

Conclusions

Worldwide climate change has been partially ascribed to fossil fuel combustion. Oxy-fuel combustion of fossil fuels and its cooperation with solid oxide fuel cell enhances the efficiency of relating operations tremendously. Oxygen separation by membrane as a cost-effect alternative to currently existing oxygen production process is being researched.

In this research, dense thin-film membrane, Pt-GDC, was prepared. Its preparation methods were investigated to optimize synthesis process in terms of stability, cost, and effectiveness.

Specifically, it is demonstrated that the particle size of GDC colloid is inversely related to the duration of sonification process. Narrow size distribution of colloidal particle could be transformed into uniform and defect free membrane layers. Platinum colloid is stabilized with PVA while its stability is possibly related to the amount of reducing agent (methanol) used. In comparison of the Pt-GDC sample, SEM characterization of the ED-PtGDC sample substantiated the porosity filling effect of the electroless deposition (ED) process. The optimal duration of the ED process was determined to be two hours to achieve optimal surface quality. Crystallite sizes of GDC and platinum phases were determined by Scherrer equation according to XRD. Scherrer equation showed that the crystallite size of platinum remained the same. Spectroscopy ellipsometry (SE) measurements were taken to analyze thickness of the membrane. A linear relationship of membrane thickness and number of GDC coatings was observed.

Characterization results showed feasibility of the synthesis of colloids for Pt-GDC membrane. The colloids produced in this work showed improvements in terms of stability and membrane quality.

References

1. Lin, Haiqing, Meijuan Zhou, Jennifer Ly, Jimmy Vu, Johannes G. Wijmans, Timothy C. Merkel, Jianyong Jin, Adam Haldeman, Earl H. Wagener, and David Rue. "Membrane-Based Oxygen-Enriched Combustion." Industrial & Engineering Chemistry Research 52.31 (2013): 10820-0834.
2. Huynh, Cuong Van, and Song-Charng Kong. "Combustion and NOx Emissions of Biomass-derived Syngas under Various Gasification Conditions Utilizing Oxygen-enriched-air and Steam." *Fuel* 107 (2013): 455-64.
3. Eriksson, Tore, and Yohannes Kiros. "Temperature Swing Adsorption Device for Oxygen-enriched Air." *Journal of Cleaner Production* 76 (n.d.): 174-79.
4. Cheng, Hongwei, Weilin Yao, and etc. "Structural Stability and Oxygen Permeability of BaCo0.7Fe0.2M0.1O3 − δ (M = Ta, Nb, Zr) Ceramic Membranes for Producing Hydrogen from Coke Oven Gas." *Fuel Processing Technology* 131 (2014): 36-44. Print.
5. Xu, Sherman J., and William J. Thomson. "Oxygen Permeation Rates through Ion-conducting Perovskite Membranes." *Chemical Engineering Science*54.17 (1999): 3839-850.
6. Lee, T. "Oxygen Permeation in Dense SrCo0.8Fe0.2O3 − δ Membranes: Surface Exchange Kinetics versus Bulk Diffusion." *Solid State Ionics*100.1-2 (1997): 77-85.
7. Hashim, S.s., A.r. Mohamed, and S. Bhatia. "Oxygen Separation from Air Using Ceramic-based Membrane Technology for Sustainable Fuel Production and Power Generation." *Renewable and Sustainable Energy Reviews* 15.2 (2011): 1284-293.
8. Smith, A.r, and J. Klosek. "A Review of Air Separation Technologies and Their Integration with Energy Conversion Processes." *Fuel Processing Technology* 70.2 (2001): 115-34
9. Chen, Yubo, Baoming Qian, Yong Hao, and Shaomin Liu. "Influence of Sealing Materials on the Oxygen Permeation Fluxes of Some Typical Oxygen Ion Conducting Ceramic Membranes." *Journal of Membrane Science* 470 (2014): 102-11. *Scicence Direct*. Web.
10. C. Chatzichristodoulou, P. Blennow, M. Søgaard, P.V. Hendriksen, M. Mogensen A. Trovarelli, P. Fornasiero (Eds.), Catalysis by Ceria Related Materials, Imperial College Press, London (2013), p. 12
11. Belousov, Valery V., Viktor A. Schelkunov, and Sergey V. Fedorov. "Oxygen-permeable In2O3–55 Wt.% δ-Bi2O3 Composite Membrane." *Electrochemistry Communications* 20 (2012): 60-62. Print.
12. H. Verweij, XLT, Nano-composite supported membranes for cost-effective O2 separation, Proposal_draft-OCRC_O2+HV (2012)

13. Liu, H., C. Xiao, Q. Huang, X. Hu, and W. Shu. "Preparation and Interface Structure Study on Dual-layer Polyvinyl Chloride Matrix Reinforced Hollow Fiber Membranes." *Journal of Membrane Science* 472 (2014): 210-21.
14. Snider, Matthew T. "INORGANIC MEMBRANES FOR CARBON CAPTURE AND POWER GENERATION." *The Ohio State University* (2015): n. pag. Web.
15. Kilner JA. Fast anion transport in solids. *Solid State Ionics* 1983; 8:201-7
16. Skinner, Stephen J., and John A. Kilner. "Oxygen Ion Conductors." Materials Today 6.3 (2003): 30-37.
17. Dr. Lynn Fuller (March 27, 2010). "Rapid Thermal Processing (RTP)"
18. Snider, Matthew. (2014). *Inorganic Membrane for Carbon Capture and Power Generation* (Unpublished doctoral dissertation). The Ohio State University, Columbus, Ohio.
19. Perdana, Indra, Boma Wikan Tyoso, I. Made Bendiyasa, Rochmadi, Sang Kompiang Wirawan, and Derek Creaser. "Effect of External Mass Transport on Permeation in a Wicke-Kallenbach Cell." Chemical Engineering Research and Design 87.10 (2009): 1438-447.
20. Djokic, Stojan S., and Pietro L. Cavallotti. "Electroless Deposition: Theory and Applications." *Modern Aspects of Electrochemistry* 48 (2010): 251.
21. Garcia-Caurel, Enric, Antonello De Martino, Jean-Paul Gaston, and Li Yan. "Application of Spectroscopic Ellipsometry and Mueller Ellipsometry to Optical Characterization." Applied Spectroscopy 67.1 (2013): 1-21.